Mechanism of and alignment effects in spin–changing collisions involving atoms in 1 P electronic states: Ca(4s5p 1 P)+noble gases

Millard H. Alexander and Brigitte Pouilly

Citation: The Journal of Chemical Physics **90**, 5373 (1989); doi: 10.1063/1.456444
View online: http://dx.doi.org/10.1063/1.456444
View Table of Contents: http://scitation.aip.org/content/aip/journal/jcp/90/10?ver=pdfcov
Published by the AIP Publishing

Mechanism of and alignment effects in spin–changing collisions involving atoms in ^1P electronic states: Ca($4s5p\ ^1P$) + noble gases

Millard H. Alexander and Brigitte Pouilly[a)]
Department of Chemistry, University of Maryland, College Park, Maryland 20742

(Received 19 December 1988; accepted 3 January 1989)

We present a detailed study of the mechanism of spin–changing transitions between ^1P and ^3P electronic states corresponding to the $nsn'p$ Rydberg state of an alkaline earth atom in collision with a structureless, spherical partner. This type of process takes place on four potential curves and involves collisional coupling between the electronic angular momentum **L** of the electronically excited atom, the spin **S** of the atom in the final ^3P state, and the orbital angular momentum l associated with the relative motion of the collision partners. We review the use of Hund's case coupling schemes in describing the collision and present a careful analysis of the initial state preparation under conditions of laser excitation in a crossed beam experiment. This underlies the development of a new statistical model for the dependence of the spin–changing cross section on the alignment of the pump laser. Finally, we describe a new technique to follow the redistribution of flux onto locally adiabatic states as the initially excited atom is approached by the closed-shell partner. This is used to show that dynamical corrections to our simple statistical model are small.

I. INTRODUCTION

There has been considerable recent interest[1–9] in elastic as well as reactive collisions involving atoms in ^1P electronic states. Leone and co-workers[2–6] have carried out a series of experimental studies of collision-induced, spin–changing transitions between the ^1P and ^3P electronic states of the $4s5p$ Rydberg levels of Ca in collisions with noble gases and closed-shell molecules. More recently, similar studies have been carried out with electronically excited Sr.[7] Since the orientation of the excited p orbital can be selected by varying the direction of the polarization vector of the laser, it is possible to study the dependence of these spin–changing transitions on the initial alignment of the orbital.

The mechanism for this type of process involves collisional coupling between the electronic angular momentum **L** of the electronically excited atom, the spin **S** of the atom in the final ^3P state, and the orbital angular momentum l associated with the relative motion of the collision partners. In addition, since the electrostatic interaction between the open-shell atom and its collision partner will depend on the orientation of the initially excited p orbital, the collision will involve more than one potential-energy curve (or surface). Another complication is the transformation between the laboratory frame, in which the laser state selection occurs, and the collision frame.

Leone and Zare and their co-workers initially used the qualitative concept of "orbital following," developed by Hertel and co-workers,[10–12] to interpret their experiments. We then presented[9] a fully quantum description of the inelastic $^1P \leftrightarrow {}^3P$ processes under investigation in Leone's group. Unfortunately, these close-coupling calculations, although yielding exact values of the relevant cross sections, offer little physical insight, in particular into the dependence of the cross sections on orbital alignment.

In the present article we shall present a new simple model for the prediction of $^1P \rightarrow {}^3P$ cross sections. This model arises from a consideration of the reflection symmetry of the states prepared during excitation with light polarized either parallel or perpendicular to the initial relative velocity vector. In developing this model we shall first make use of Hund's case coupling schemes,[13–22] which are known[16–22] to serve as a useful guide in constructing the proper basis to describe the collision both at large and small values of the interatomic separation. Then we shall describe a new way to examine the evolution during the collision of the initially prepared state. This is done by inward propagation of the full wave function for the system and then projecting the flux onto a locally adiabatic basis. This procedure gives additional insight into the extent to which the orbital "follows"[10–12] during the collision.

The organization of the present article is as follows: Section II contains a brief review, taken from our earlier work,[9,23] of the use of Hund's case coupling schemes in describing the atom–atom collisions under consideration here. Section III follows with a review of the quantum formulation of the scattering dynamics. A detailed analysis of the initial state preparation is contained in Sec. IV. This underlies the development of a new statistical model for the observed alignment effects, which is described in Sec. V. Then, in Sec. VI, we discuss how we follow the redistribution of flux as the initially excited Ca atom approaches a closed-shell partner. Section VII contains a short discussion of "orbital locking" models in light of the present study. A brief conclusion follows. The Appendix contains the details of the flux propagation technique used in Sec. VI.

II. SYSTEM WAVE FUNCTIONS, HUND'S CASE COUPLING SCHEMES, AND SYMMETRY DESIGNATION

Consider the collision between an open-shell atom and a closed-shell atomic partner. Let **R** designate the interatomic distance (the bond axis of the diatomic) and let **r** designate

[a)] NATO Science Fellow, 1987. Permanent address: Laboratoire de Spectroscopie des Molécules Diatomiques, URA 779, Université de Lille Flandres-Artois, Bâtiment P5, 59655 Villeneuve d'Ascq Cedex, France.

 0021-9606/89/105373-13$02.10

the coordinates of the electrons. The total Hamiltonian of the diatomic system can be written as

$$H(\mathbf{R},\mathbf{r}) = -\frac{\hbar^2}{2\mu R^2}\frac{d}{dR}R^2\frac{d}{dR} + H_{\rm rot}(\hat{R}) + V(R,\mathbf{r}) + V_{\rm fs}(R,\mathbf{r}), \quad (1)$$

where μ is the collision reduced mass and $V_{\rm fs}(R,\mathbf{r})$ is the fine-structure Hamiltonian for the open-shell atom. Here $H_{\rm rot}(\hat{R})$ is the Hamiltonian for the orbital motion of the two nuclei, namely

$$H_{\rm rot}(\hat{R}) = \frac{\hbar^2}{2\mu R^2}l^2 = \frac{\hbar^2}{2\mu R^2}(\mathbf{J}-\mathbf{L}-\mathbf{S})^2, \quad (2)$$

where $\mathbf{L}$, $\mathbf{S}$, l, and $\mathbf{J}$ denote, respectively, the electronic orbital and spin angular momenta of the open–shell atom, the orbital angular momentum of the two nuclei, and the total angular momentum. In Eq. (1) $V(R,\mathbf{r})$ designates the total electronic Hamiltonian, independent of spin–orbit, spin–spin, or hyperfine coupling, namely

$$V(R,\mathbf{r}) = H_0(\mathbf{r}) + W(R,\mathbf{r}), \quad (3)$$

where $H_0(\mathbf{r})$ represents the *electronic* Hamiltonian (again exclusive of spin-dependent terms) of the isolated atoms. The term $W(R,\mathbf{r})$ is the electrostatic interaction which arises as the two atomic collision partners approach. We assume that $W(R,\mathbf{r})$ vanishes as $R\to\infty$.

Asymptotically, when the separation between the collision partners is so large that the electrostatic interaction potential is negligibly small, the wave function of the combined system is most conveniently expanded in an *uncoupled* basis, namely a product of the wave function of the open-shell atom, $|LSjm_j\rangle$, multiplied by the wave function which describes the relative orbital motion of the two collision partners, $|lm_l\rangle$. Here $\mathbf{j}=\mathbf{L}+\mathbf{S}$ is the total angular momentum of the open-shell atom and m_j and m_l denote the projections of $\mathbf{j}$ and l, respectively, along the space-fixed Z axis.

In an actual scattering calculation it is more convenient to work with states which are eigenfunctions of the total angular momentum $\mathbf{J}$.[9,20,21,23–25] These states, which correspond to Hund's case (e) coupling,[13,19,25] can be obtained by vector coupling the $|LSjm_j\rangle|lm_l\rangle$ states, namely[26]

$$|LSjlJM\rangle = \sum_{m_j m_l}(jm_j lm_l|JM)|LSjm_j\rangle|lm_l\rangle, \quad (4)$$

where $(\cdots|\cdots)$ is a Clebsch–Gordan coefficient and M is the projection of $\mathbf{J}$ along a space-fixed Z axis.

For the interaction between a closed-shell atom and an atom in a ^{2S+1}P electronic state the parity of these Hund's case (e) wave functions is *independent* of j and given by

$$i|LSjlJM\rangle = (-1)^{n+l}|LSjlJM\rangle, \quad (5)$$

where n denotes the number of p electrons. In modern spectroscopic notation states of *odd* multiplicity with parity $(-1)^J$ are labeled e and states with parity $-(-1)^J$ are labeled f.[27] The correlation between the j, l, and J quantum numbers and the e/f label is clarified by Table I. We note, in particular, that the unique $S=1, j=0$ fine-structure level is f labeled.

In the case (e) basis the matrix elements of *both* the rotational and spin–orbit Hamiltonians are diagonal and given by[9,23]

$$\langle L'S'j'l'JM|H_{\rm rot}|LSjlJM\rangle = \delta_{LL'}\delta_{SS'}\delta_{ll'}\delta_{jj'}\hbar^2 l(l+1)/(2\mu R^2) \quad (6)$$

and

$$\langle L'S'j'l'JM|V_{\rm fs}|LSjlJM\rangle = \delta_{ll'}[\delta_{jj'}\delta_{S1}\delta_{S'1}\tfrac{1}{2}a_3(R)j(j+1) + \delta_{j1}\delta_{j'1}(1-\delta_{SS'})a_{13}(R)], \quad (7)$$

Here $a_3(R)$ denotes the spin–orbit coupling within the ^3P state and $a_{13}(R)$ denotes the off-diagonal (in S) spin–orbit coupling between the ^1P and ^3P states.

In the case (e) basis the electronic Hamiltonian is *not* diagonal. The matrix elements are[9,23]

$$\langle L'S'j'l'JM|W(R,\mathbf{r})|LSjlJM\rangle = \delta_{SS'}\delta_{ll'}\delta_{jj'}[{}^{2S+1}W_\Pi(R)+\delta_{S1}\Delta E_{13}] + [ll'jj']^{1/2}\times[{}^{2S+1}W_\Sigma(R)-{}^{2S+1}W_\Pi(R)]\sum_\Omega \times\begin{pmatrix} l & j & J\\ 0 & \Omega & -\Omega\end{pmatrix}\begin{pmatrix} l' & j' & J\\ 0 & \Omega & -\Omega\end{pmatrix}\begin{pmatrix} L & S & j\\ 0 & \Omega & -\Omega\end{pmatrix}\begin{pmatrix} L & S & j'\\ 0 & \Omega & -\Omega\end{pmatrix}, \quad (8)$$

TABLE I. Association of quantum numbers and e/f labels for states arising from the interaction of a closed-shell atom with an atom with an *odd* number of p electrons in a ^{2S+1}P electronic state.

	e levels	f levels
	Case (e) wave functions (parity and e/f label independent of j)	
$S=0$	$j=1, l=J-1, J+1$	$j=1, l=J$
$S=1$	⋯	$j=0, l=J$
	$j=1, l=J-1, J+1$	$j=1, l=J$
	$j=2, l=J-1, J+1$	$j=2, l=J-2, J, J+2$
	Case (a) wave functions	
$S=0$	$^1\Sigma_0^+$, $^1\Pi_1(\epsilon=+1)$	$^1\Pi_1(\epsilon=-1)$
$S=1$	$^3\Sigma_1^+(\epsilon=-1)$, $^3\Pi_{0,1,2}(\epsilon=-1)$	$^3\Sigma_0^+$, $^3\Sigma_1^+(\epsilon=+1)$, $^3\Pi_{0,1,2}(\epsilon=+1)$

where $(:::)$ is a $3j$ symbol[26] and $[x_1x_2\cdots x_n] = (2x_1+1)(2x_2+1)\cdots(2x_n+1)$ denotes a product of angular momentum rotational degeneracy factors. Here ${}^{2S+1}W_\Pi(R)$ and ${}^{2S+1}W_\Sigma(R)$ designate the electronically adiabatic potential curves of Π and Σ symmetry which arise when, as discussed above, the spatial degeneracy of the unfilled p orbital is lifted by the approach of the closed-shell partner. It is these curves which would result from an *ab initio* or pseudopotential calculation of the electronic potential curves of the diatomic system.[28–30] The quantity ΔE_{13} represents the splitting between the ${}^1P$ and ${}^3P_{j=0}$ levels of the isolated atom. For simplicity, in the discussion below we shall suppress the electronic orbital momentum L in the designation of the case (e) wave functions, except where it is explicitly needed. Note that the matrix elements in Eq. (8) are independent of the projection quantum number M.

For interactions involving an atom in a ${}^{2S+1}P$ state with a closed-shell atom, we anticipate that the Σ curve will be more repulsive at short range. The *qualitative* behavior of these Σ and Π potential curves is illustrated in Fig. 1, where we have plotted two sets of Σ and Π curves, assuming that these arise from the same electron occupancy of the open-shell atom (as, for example, the $4s5p\ {}^1P$ and $4s5p\ {}^3P$ states of the Ca atom).

The case (e) description is most appropriate at long range, where the electrostatic interaction is negligibly small compared to either the centrifugal potential or the spin–orbit coupling. Thus, in the case (e) basis the Hamiltonian becomes asymptotically diagonal except for the residual mixing between the ${}^1P$ and ${}^3P_{j=1}$ states, arising from the off-diagonal spin–orbit coupling $a_{13}(R=\infty)$. One can fully diagonalize the Hamiltonian by working with a linear combination of these two $j=1$ states, namely

$$|F_0 jlJM\rangle = \cos\theta\,|S=0,jlJM\rangle + \sin\theta\,|S=1,jlJM\rangle \quad (9)$$

and

$$|F_1 jlJM\rangle = -\sin\theta\,|S=0,jlJM\rangle + \cos\theta\,|S=1,jlJM\rangle, \quad (10)$$

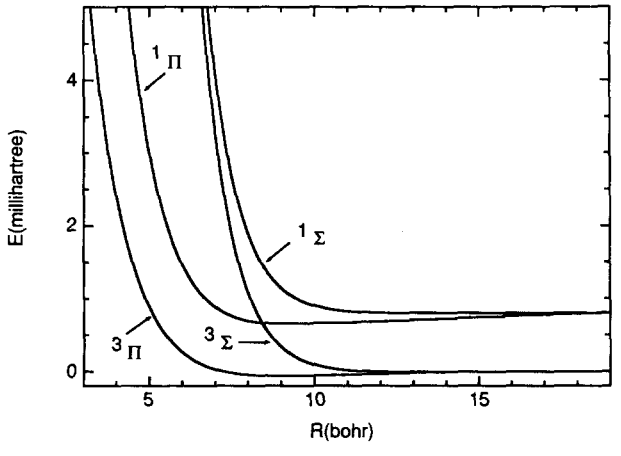

FIG. 1. Typical potential-energy curves of ${}^1\Sigma$, ${}^3\Sigma$, ${}^1\Pi$, and ${}^3\Pi$ symmetry which would arise from the interaction of a closed-shell atom with an atom in $(...nsn'p\ {}^1P)$ and $(...nsn'p\ {}^3P)$ electronic states. The actual potential-energy curves shown are appropriate to the interaction of $Ca(4s5p)$ with He and are identical to those defined as "set III" in Table II of Ref. 9.

where the rotation angle is defined by

$$\theta = \tfrac{1}{2}\tan^{-1}\{2a_{13}(\infty)/[E({}^1P_1) - E({}^3P_1)]\}. \quad (11)$$

In the limit of small mixing the $|F_0\rangle$ state is nominally singlet and the $|F_1\rangle$ state, nominally triplet. Since the spin–orbit mixing is independent of l, so will be the rotation angle θ. In collisions involving a closed-shell partner, where the interaction involves no bond formation, it is reasonable to assume that the off-diagonal spin–orbit coupling in the open-shell atom $[a_{13}(R)]$ varies little from its asymptotic value, at least at moderate to large value of R.[29] Thus, the rotation angle θ will be virtually independent of R. We can extend the F_S labeling to include the two triplet states which are not mixed with the ${}^1P_1$ state by defining, for $j\neq 1$

$$|F_1, j\neq 1, lJM\rangle = |S=1, j\neq 1, lJM\rangle. \quad (12)$$

The matrix elements of $H_{\rm rot}$, $V_{\rm fs}$, and $W(R,\mathbf{r})$ in the F_S basis correspond to the matrix elements in Eqs. (6)–(8), with the exception that the matrix elements involving states with $j=1$ must be further transformed in accordance with Eqs. (9) and (10).

Since $H_{\rm rot}$ is diagonal in the case (e) basis, and since the transformation to the F_S basis is diagonal in I, this operator remains diagonal with matrix elements given by Eq. (6). However, the transformation to the F_S basis will give rise to matrix elements of the electrostatic potential which couple states which correlate to the ${}^1P$ and ${}^3P$ asymptotes. It is these terms which give rise to the singlet→triplet transitions observed experimentally by Leone and co-workers[2–6] in collisions of $Ca(4s5p\ {}^{1,3}P)$.

At close interparticle separation, the splitting between the Σ and Π potential curves will become larger than the rotational or spin–orbit terms in the Hamiltonian. In this close-in, molecular region it is natural to use a basis in which the electrostatic Hamiltonian is diagonal. This is the Hund's case (a) basis, with wave functions designated ${}^{2S+1}\Lambda_\Omega$ and given by[9,15,31]

$$|\Lambda S\Sigma\Omega\epsilon JM\rangle = 2^{-1/2}(|\Lambda S\Sigma\rangle|JM\Omega\rangle + \epsilon|-\Lambda,S,-\Sigma\rangle|JM,-\Omega\rangle). \quad (13)$$

Here Λ and Σ denote the projections of $\mathbf{L}$ and $\mathbf{S}$ along the molecular axis $(\mathbf{R})$, and $\Omega=\Lambda+\Sigma$. The symmetry index ϵ can take on the values ± 1 except for the ${}^3\Sigma_0^+$ and ${}^1\Sigma^+$ states where $\Lambda=\Sigma=\Omega=0$ and the wave functions are written as

$$|\Lambda=0,S,\Sigma=\Omega=0,J,M\rangle = |\Lambda=0,S,\Sigma=0\rangle|JM0\rangle. \quad (14)$$

In the case (a) basis L, j, and l are no longer good quantum numbers;[14,15] they are replaced by Λ, Σ, Ω, and ϵ. In this case (a) basis the electrostatic Hamiltonian is diagonal with matrix elements[9,23]

$$\langle\Lambda'S'\Sigma'\Omega'\epsilon'JM|W(R,\mathbf{r})|\Lambda S\Sigma\Omega\epsilon JM\rangle = \delta_{\Lambda\Lambda'}\delta_{SS'}\delta_{\Sigma\Sigma'}\delta_{\Omega\Omega'}\delta_{\epsilon\epsilon'}\,{}^{2S+1}W_\Lambda(R). \quad (15)$$

One can show that for states arising from the interaction between a closed-shell atom and a ${}^1P$ atom the parity of the

case (a) states is $\epsilon(-1)^{J-S}$, except for the $^{1,3}\Sigma_0^+$ states, with parity $(-1)^{J-S}$.[32] Thus for $S=0$ the $\epsilon=+1\,^{2S+1}\Lambda_\Omega$ states are labeled e and the $\epsilon=-1\,^{2S+1}\Lambda_\Omega$ states, f, except for the unique $^1\Sigma_0^+$ state [Eq. (14)] which is labeled e. By contrast, for $S=1$ the $\epsilon=-1\,^{2S+1}\Lambda_\Omega$ states are labeled e and the $\epsilon=+1\,^{2S+1}\Lambda_\Omega$ states, f, except for the unique $^3\Sigma_0^+$ state [Eq. (14)] which is labeled f. The connection between the e/f labeling and the case (a) quantum numbers is summarized in Table I. The relation between the case (e) and case (a) wave functions has been given previously.[20,21]

III. QUANTUM FORMULATION OF THE COLLISION DYNAMICS

In the standard close-coupled treatment of the collision dynamics the total wave functions is expanded in terms of the case (e) wave functions, namely

$$Y(\mathbf{R},\mathbf{r})=\sum_{JMSjl}\frac{1}{R}C^{JM}_{Sjl}(R)|F_Sjl JM\rangle. \tag{16}$$

Here we assume that proper linear combinations of the $j=1$, $S=1$, and $j=1$, $S=0$ basis states have been taken in order to diagonalize the off-diagonal spin–orbit coupling term [see Eqs. (9)–(11)]. The expansion coefficients in Eq. (16) satisfy the usual close-coupled (CC) equations, which are diagonal in the total angular momentum J.[20,24,25,28,30,33–36]

Within the usual close-coupled formulation, the Schrödinger equation is solved by expansion of the wave function in the asymptotic [case (e)] basis.[9,23,25] This basis can be designated a *diabatic* basis, since it is *independent* of the interparticle separation. Other diabatic bases are possible, for example, a case (a) basis. The advantage of the case (e) basis is that the Hamiltonian is diagonal asymptotically, so that the close-coupled equations become uncoupled as $R\to\infty$.

Alternatively, one can expand the total wave functions in an *adiabatic* basis.[16,20,21,37–40] This basis is defined by an orthogonal transformation of the diabatic basis, namely

$$|nJM;R\rangle=\sum_{Sjl}A^{JM}_{n,Sjl}(R)|F_Sjl JM\rangle, \tag{17}$$

where the index n ranges over all the states in the coupled ($|F_Sjl JM\rangle$) case (e) basis. The transformation matrix is chosen to diagonalize the matrix of the total Hamiltonian

$$\mathbf{A}(R)\mathbf{U}^J(R)\mathbf{A}^T(R)=\lambda^J(R), \tag{18}$$

where $\mathbf{U}^J(R)\equiv U^J_{F'_Sj'l',F_Sjl}(R)$ is defined as[9,23]

$$U^J_{F'_Sj'l',F_Sjl}(R)=\langle F'_Sj'l'JM|H_{\rm rot}+V_{\rm fs}+W(R,\mathbf{r})|F_Sjl JM\rangle. \tag{19}$$

The eigenvalues of the transformation, $\lambda^J(R)$, are the adiabatic energies. The adiabatic basis is *unique*; each choice of diabatic basis will result in a different transformation matrix $\mathbf{A}$, but the resulting adiabatic states $|nJM\rangle$ will be the same. Note also that the transformation is *independent* of the total energy. For a value of the total angular momentum $J=2$, the adiabatic energies of the six e-labeled states [parity $(-1)^J$], are plotted in Fig. 2 and, enlarged, in the upper panel of Fig. 3. The asymptotic correlation between these adiabatic states and the appropriate case (e) and case (a) states is given in Table II. It is worthwhile observing that the $^3\Sigma_1^+$ case (a) state with $\Omega=1$ correlates asymptotically with the *singlet* $^1P_1$ case (e) state with $l=J-1$ and, conversely the $^1\Pi_1$ case (a) state correlates with the *triplet* $^3P_2$ case (e) state with $l=J+1$. The strong avoided crossing between the $^3\Sigma$ and the $^1\Pi$ electrostatic potential curves (Fig. 1) is clearly apparent; remember that the $^1P_1$ and $^3P_1$ atomic states are mixed slightly by the spin–orbit Hamiltonian (see Sec. II).

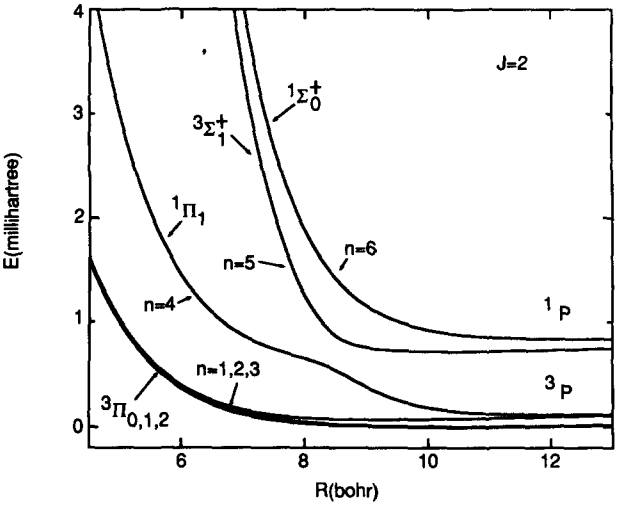

FIG. 2. Adiabatic energies [λ^J, Eq. (18)] of the six e-labeled states which correlate asymptotically to the diabatic [case (e)] states corresponding to the interaction of an atom in ^1P and ^3P electronic states with a closed-shell atom. The curves were calculated using the $^1\Sigma$, $^3\Sigma$, $^1\Pi$, and $^3\Pi$ potential curves shown in Fig. 1 for a total angular momentum of $J=2$ and assuming a mixing angle of $\theta=18.4°$ ($\sin^2\theta=0.1$). The correlation between the six adiabatic states and the case (e) and case (a) states is given in Table II. The curves for the lowest two adiabatic states are virtually indistinguishable.

The major contribution to $^1P\to{}^3P$ cross sections will arise from collisions at impact parameters at which the clas-

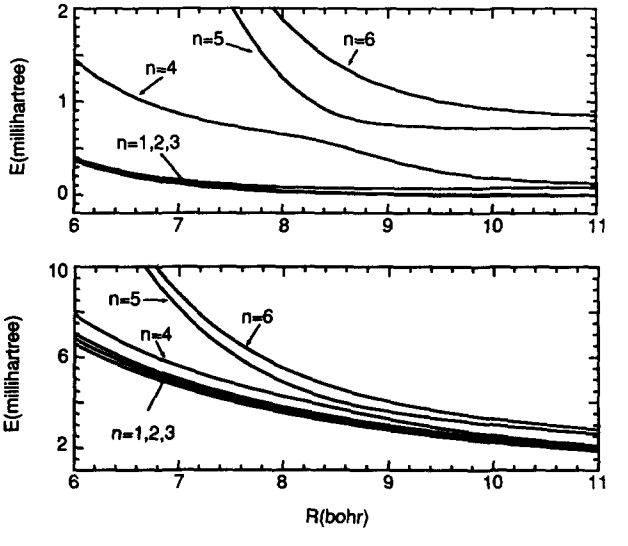

FIG. 3. (Upper panel) Enlargement of the adiabatic energies shown in Fig. 2. (Lower panel) identical set of adiabatic energies calculated for a total angular momentum of $J=55$.

TABLE II. Correlation of adiabatic and diabatic [case (e) or case (a)] e-labeled states.

Case (e)					Case (e)				
n	S	j	l	Case(a)	n	S	j	l	Case(a)
1	1	1	$J-1$	$^3\Pi_0$	5	0	1	$J-1$	$^3\Sigma_1^+$
2	1	1	$J+1$	$^3\Pi_1$	6	0	1	$J+1$	$^1\Sigma_0^+$
3	1	2	$J-1$	$^3\Pi_2$					
4	1	2	$J+1$	$^1\Pi_1$					

sical turning point is roughly equal to the point of crossing between the $^3\Sigma$ and the $^1\Pi$ potential curves (Fig. 1). For Ca–He collisions at an energy of 0.1 eV and an impact parameter of ~ 8.5 bohr (which is roughly equal to the $^3\Sigma - {}^1\Pi$ crossing in Fig. 1), the corresponding nuclear orbital angular momentum is ~ 55. The adiabatic potentials for $J = 55$ are shown in the lower panel of Fig. 3. The presence of the large centrifugal barrier obscures both the overall difference between the nominally Σ and the nominally Π adiabatic potential curves at moderate to large values of R as well as the avoided crossing between the nominally $^3\Sigma$ and the nominally $^1\Pi$ curves.

IV. INITIAL STATE PREPARATION

The analysis of beam experiments involving laser preparation of an atom in an excited ^1P electronic state is considerably more complex than that of an experiment in which one measures only degeneracy averaged cross sections. Imag ine an experiment involving two perpendicular atomic beams and a pump laser at right angles to both beams, as illustrated schematically in Fig. 4. We shall assume that the laser is *linearly* polarized, and that the electric field vector of the laser defines the laboratory frame Z axis. Thus, in a $^1P \leftarrow {}^1S$ excitation, only the $m_L = 0$ projection level will be prepared. The general quantum analysis of the collision refers to a coordinate system with z-axis defined by the initial relative velocity vector—the so-called collision frame.[33] This frame, which is *fixed* in space, must be distinguished both from the laboratory frame as well as from the molecular frame, whose origin is fixed at the center of mass of the molecule and whose z axis is defined by **R**, the relative separation vector. The collision frame and the molecular frame coincide, in general, only prior to the collision.

Although it is most convenient to carry out the scattering calculation in a *coupled* basis (Sec. II) in which the total angular momentum is a good quantum number, the wave function of two atoms at infinite separation can be expressed most simply in an *uncoupled* basis. Prior to the collision the relative orbital angular momentum l of the diatomic (atom + laser-excited atom) is always oriented perpendicular to the collision plane, and, consequently, perpendicular to the collision-frame z axis, which is coincident with $\mathbf{v}_{rel}$, the initial relative velocity vector. In the case of *parallel* excitation, the laboratory fixed Z axis, which is defined by the electric field vector of the pump laser, will lie parallel to $\mathbf{v}_{rel}$. Since $\hat{Z}$ and $\mathbf{v}_{rel}$ are coincident prior to the collision, the collision frame and laboratory frame z axes are identical. Nevertheless, the *azimuthal* orientation of l with respect to $\hat{Z}$ is not restricted—a unique collision plane is not selected. This is shown clearly in Fig. 5.

In the case of perpendicular excitation the electric field vector of the pump laser **E** is perpendicular to $\mathbf{v}_{rel}$ (Fig. 4). However, as shown clearly in Fig. 6, although both l and **E** must lie perpendicular to $\mathbf{v}_{rel}$, the angle between l and **E** is *unrestricted*. Consequently, the orientation of the initially excited p orbital with respect to the collision plane is also unrestricted. That a unique collision plane is not seclected occurs because when a definite value is assigned to the orbital angular momentum l and its projection m_l, the conjugate angle—the azimuthal orientation of the collision plane—becomes totally undetermined.

In the case of parallel excitation only the $^1P_{m_j=0}$ ($|j=1, m_j=0\rangle$) atomic state is prepared.[13–15,41] Since the prepared p orbital has $m_L = 0$, it lies along $\mathbf{v}_{rel}$ and is perpendicular to l. Furthermore, since l is perpendicular to $\mathbf{v}_{rel}$ and, hence, perpendicular to $\hat{Z}$, m_l must be zero. Thus only the $|j=1, m_j=0\rangle|l, m_l=0\rangle$ *uncoupled* state is prepared. This initially prepared state, which we shall designate $|1_\parallel\rangle$, can be ex-

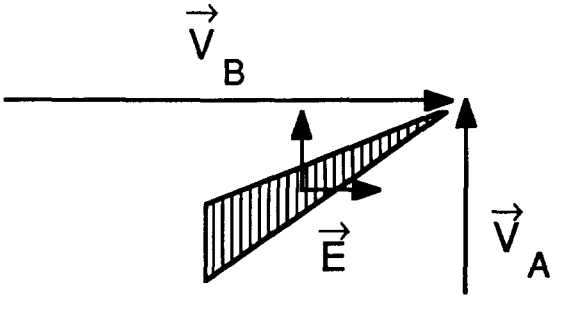

FIG. 4. Schematic representation of two atomic beams crossing at right angles intersected at right angles by a linearly polarized laser beam. The electric field vector of the laser can be rotated in the plane defined by the two atomic beams.

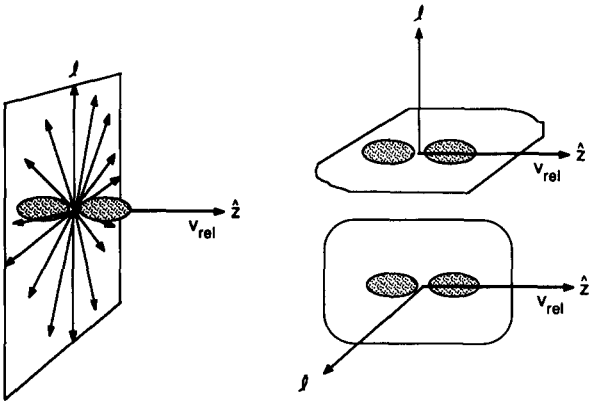

FIG. 5. Schematic representation of the initial relative velocity vector $\mathbf{v}_{rel}$, the initial relative orbital angular momentum l, and the initially excited p orbital in the case of parallel excitation. Since the prepared p orbital has $m_L = 0$, it lies along $\mathbf{v}_{rel}$ and thus is always perpendicular to l. Yet, although $\hat{Z}$ and v_{rel} are coincident prior to the collision, the *azimuthal* orientation of l is not restricted—a unique collision plane is not selected. Since the initially excited p orbital always lies perpendicular to l, and hence in the plane of rotation, only a Σ state is prepared.

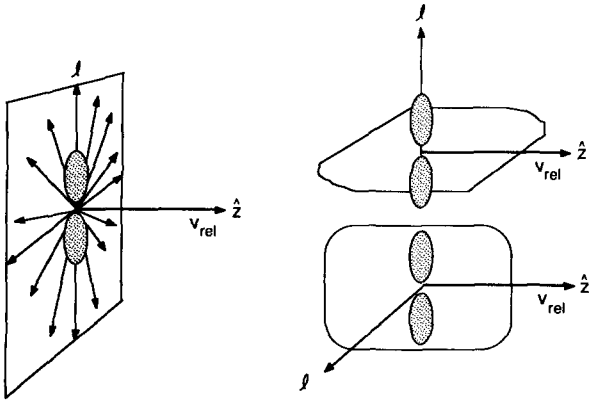

FIG. 6. Schematic representation of the initial relative velocity vector $\mathbf{v}_{rel}$, the initial relative orbital angular momentum l, and the initially excited p orbital in the case of perpendicular excitation. Since the prepared p orbital has $m_L = \pm 1$, it lies perpendicular to $\mathbf{v}_{rel}$ but is not necessarily perpendicular to l. Yet, although $\hat{Z}$ and $\mathbf{v}_{rel}$ are coincident prior to the collision, the *azimuthal* orientation of l is not restricted—a unique collision plane is not selected. Also, the initially prepared p orbital can be either perpendicular to or in the plane of collision. Thus the initially excited electronic wave function can be either symmetric or antisymmetric with respect to reflection in the initial plane of rotation of the two atom system—both $\Pi(A')$ and $\Pi(A'')$ Λ-doublet states are prepared.

pressed as a linear combination of *two* coupled [case (e)] wave functions corresponding to *two* values of the total angular momentum J. By reversing the angular momentum coupling[26] contained in Eq. (4) we find

$$|1_{\|}\rangle = (10l0|l+1,0)|S=0,j=1,l,J=l+1,M=0\rangle + (10l0|l-1,0)|S=0,j=1,l,J=l-1,M=0\rangle. \quad (20)$$

We observe (see Table I) that the two coupled states which are prepared are both e levels. Alternatively, one can discuss the initial state preparation in terms of case (a) wave functions. Since the prepared orbital has $m_L = 0$ (with respect to $\hat{Z}$) and since $\hat{Z}$ and $\mathbf{v}_{rel}$ coincide prior to the collision, only a molecular state of $^1\Sigma$ symmetry is prepared, which is e labeled.

The correct mechanistic interpretation of the collision dynamics in this case of parallel excitation will then involve the study of the evolution of this initially prepared state as the collision partners approach. The total angular momentum J and its projection M are conserved during the collision, and the Hamiltonian will not mix e and f levels. Hence, for a given value of I only e levels with $J = l \pm 1$ will mix with the $|1_{\|}\rangle$ state. There are only *three* other *singlet* states which meet these criteria, which we designate $|i_{\|}\rangle$, with $i = 2, 3, 4$.

The four e labeled states which are coupled together can be written as linear combination of the following case (e) states $\{\phi_k^l\}$, namely,

$$\phi_1^l = |l,J=l-1,M=0\rangle, \quad (21a)$$

$$\phi_2^l = |l,j=l+1,M=0\rangle, \quad (21b)$$

$$\phi_3^l = |l+2,J=l+1,M=0\rangle, \quad (21c)$$

$$\phi_4^l = |l-2,J=l-1,M=0\rangle. \quad (21d)$$

On the right-hand sides of Eqs. (21) and in the text which follows, we have for simplicity suppressed the value of $S(S=1)$ and $j(j=1)$ in writing the case (e) states. The expansion of the four states (state $|1_{\|}\rangle$ plus three orthogonal states) which are involved in the case of parallel excitation $|i_{\|}\rangle$ in terms of the ϕ_k^l states can be written in matrix notation as

$$|i_{\|}\rangle = \{\phi_k^l\}\mathbf{C}_{\|}^l, \quad (22)$$

where the matrix $\mathbf{C}_{\|}^l$ is given in Table III.

Insight can be gained by diagonalizing the full Hamiltonian in the basis formed by states $|i_{\|}\rangle$. At large R, the primary coupling will involve these four singlet states, since the triplet states will be well separated energetically. It is important to notice that states $|1_{\|}\rangle$ and $|2_{\|}\rangle$ have the *same* value of l and thus will become degenerate asymptotically, when the difference between $^1W_\Sigma(R)$ and $^1W_\Pi(R)$ becomes negligibly small compared to the centrifugal barrier. In fact, the wave function for state $|2_{\|}\rangle$, expressed in an *uncoupled* basis, is

$$|2_{\|}\rangle = 2^{-1/2}[|j,m_j=+1\rangle|l,m_l=-1\rangle + |j,m_j=-1\rangle|l,m_l=+1\rangle]. \quad (23)$$

This corresponds to a state in which the p orbital is no longer aligned parallel to $\mathbf{v}_{rel}$, in other words asymptotically state $|2_{\|}\rangle$ corresponds to a $^1\Pi_{1e}(\epsilon=+1)$ molecular state.

Since states $|i_{\|}\rangle$ are linear combinations of case (e) states, the off-diagonal coupling will be due solely to the electrostatic Hamiltonian. The matrix of the electrostatic Hamiltonian in the $|i_{\|}\rangle$ basis can be obtained from Eq. (8) and is given explicitly in Table IV. We observe that the off-diagonal matrix elements are *all* proportional to $^1W_\Sigma(R) - {}^1W_\Pi(R)$. In addition, with the exception of the $\langle 1_{\|}|W|2_{\|}\rangle$ matrix element, *all* the matrix elements become independent of l as l becomes large. The $\langle 1_{\|}|W|2_{\|}\rangle$ matrix element decreases as $1/l$ in the large-l limit. However, since states $|1_{\|}\rangle$ and $|2_{\|}\rangle$ become degenerate asymptotically, even for large l (large impact parameter) the electrostatic mixing will cause them to mix strongly.

Compared to state $|1_{\|}\rangle$, state $|2_{\|}\rangle$ represents a reorientation of *both* the p orbital as well as the orbital angular momentum. This reorientation is accomplished by rotation of $\mathbf{L}$ and l in an opposite sense, so that the total projection quantum number $(M = m_j + m_l)$ remains 0. Thus, the asymptotic mixing of states $|1_{\|}\rangle$ and $|2_{\|}\rangle$ will lead to a scrambling of the initially prepared orientation of the p orbital. There is another implication: In many semiclassical treatments of atomic and molecular collisions both the orientation and the magnitude of l are assumed to remain *fixed* during the collision.[39,42,43] The discussion here casts serious

TABLE III. Transformation matrix $\mathbf{C}_{\|}^l$ for parallel excitation.

$-\{l/(2l+1)\}^{1/2}$	$\{(l+1)/(2l+1)\}^{1/2}$	0	0
$\{(l+1)/(2l+1)\}^{1/2}$	$\{l/(2l+1)\}^{1/2}$	0	0
0	0	1	0
0	0	0	1

TABLE IV. Matrix elements of the electrostatic Hamiltonian in the singlet basis defined by Table II and Eq. (21).[a]

$\|1_\parallel\rangle$	$\|2_\parallel\rangle$	$\|3_\parallel\rangle$	$\|4_\parallel\rangle$
$W_{\Pi}+\Delta\frac{2l^2+2l+1}{(2l-1)(2l+3)}$	$-\Delta\frac{[l(l+1)]^{1/2}}{(2l-1)(2l+3)}$	$-\Delta\frac{l+1}{2l+3}\left[\frac{l+2}{2l+1}\right]^{1/2}$	$-\Delta\frac{l}{2l-1}\left[\frac{l-1}{2l+1}\right]^{1/2}$
	$W_{\Pi}+\Delta\frac{2l(l+1)}{(2l-1)(2l+3)}$	$\frac{-\Delta}{2l+3}\left[\frac{l(l+1)(l+2)}{2l+1}\right]^{1/2}$	$\frac{-\Delta}{2l-1}\left[\frac{l(l-1)(l+1)}{2l+1}\right]^{1/2}$
		$W_{\Pi}+\Delta\frac{(l+2)}{(2l+3)}$	0
			$W_{\Pi}+\Delta\frac{(l-1)}{(2l-3)}$

[a] The quantity Δ denotes ${}^1W_\Sigma(R)-{}^1W_\Pi(R)$.

doubts on the validity of this approximation (and, consequently, on the accuracy of cross sections calculated by this type of semiclassical method), since the mixing between states $|1_\parallel\rangle$ and $|2_\parallel\rangle$ cannot occur if the orientation of l is assumed to remain *fixed*.[44]

An alternative picture involves a case (a) basis. As discussed above, the initially prepared state corresponds to a ${}^1\Sigma_e$ molecular state. At large R, this state becomes degenerate (Fig. 1) with a ${}^1\Pi$ molecular state. Because of this degeneracy the $\mathbf{J}\cdot\mathbf{L}$ term in the rotational Hamiltonian [Eq. (2)] will strongly couple this ${}^1\Sigma$ state and the e labeled ($\epsilon=+1$) component of the ${}^1\Pi$ state.

The four singlet adiabatic energies (obtained by diagonalization within the basis formed by states $|i_\parallel\rangle$) are shown in Fig. 7. We shall denote the corresponding adiabatic states by $\Psi_{k\parallel}$. Here we have taken the electrostatic potential-energy curves ${}^1W_\Sigma(R)$ and ${}^1W_\Pi(R)$ from Fig. 1 and used $l=10$.

As R decreases, the curves separate into two pairs, which correlate at short range with, respectively, the ${}^1W_\Sigma(R)$ and ${}^1W_\Pi(R)$ curves in Fig. 1. For a given value of J there is one Σ-like and one Π-like adiabatic e-labeled curve which correlate with ${}^1P$ asymptote. For both values of J the case (e) state with $l=J-1$ correlates with the Π-like curve and the case (e) state with $l=J+1$, with the Σ-like curve. We notice, in particular, that since both the initially prepared state $|1_\parallel\rangle$ as well as the state $|2_\parallel\rangle$ are linear combinations of a case (e) state with $l=J+1$ and a state with $l=J-1$ (Table III), both states $|1_\parallel\rangle$ and $|2_\parallel\rangle$ will correlate at shorter distance with one Σ-like and one Π-like curve. Since states $|1_\parallel\rangle$ and $|2_\parallel\rangle$ are directly coupled by the electrostatic Hamiltonian, the state initially prepared in an experiment with parallel excitation (state $|1_\parallel\rangle$) will inescapably correlate with *equal probability* with the case (a) ${}^1\Pi$ and ${}^1\Sigma$ curves. As we will see in Sec. V below, as the two collision partners approach, flux initially associated with the state does split equally among the case (a) ${}^1\Pi$ and ${}^1\Sigma$ curves.

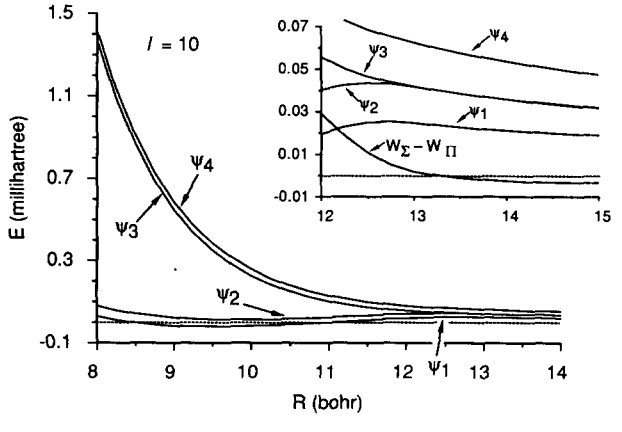

FIG. 7. Adiabatic energies of the four e-labeled states (denoted Ψ_k) which correlate asymptotically to the four uncoupled basis states $|i_\parallel\rangle$ defined by Eq. (22) for an orbital angular momentum of $l=10$. The inset shows in more detail the coalescence of the $|1\rangle$ and $|2\rangle$ states at long distance. Also shown in the inset is the splitting between the ${}^1\Sigma$ and ${}^1\Pi$ curves at long range.

Let us turn now to an examination of the situation where the polarization vector of the excitation laser is perpendicular to $\mathbf{v}_{\rm rel}$. Without loss of generality we can take $\mathbf{E}\|\hat{X}$. In this case the ${}^1P_x$ atomic state will be prepared, with wave function $2^{-1/2}(-|m_L=1\rangle+|m_L=-1\rangle)$. Again, the wave function of two atoms at infinite separation can be best be expressed in an *uncoupled* basis, namely

$$|1_\perp\rangle=2^{-1/2}[-|j=1,m_j=1\rangle|l,m_l=0\rangle + |j=1,m_j=-1\rangle|l,m_l=0\rangle], \tag{24}$$

or in a coupled [case (e)] basis as

$$\begin{aligned}|1_\perp\rangle=2^{-1/2}[&-(11l0|l+1,1)|l,J=l+1,1\rangle\\&-(11l0|l1)|l,J=l,1\rangle\\&-(11l0|l-1,1)|l,J=l-1,1\rangle\\&+(1-1l0|l+1,-1)|l,J=l+1,-1\rangle\\&+(1-1l0|l,-1)|l,J=l,-1\rangle\\&+(1-1l0|l-1,-1)|l,J=l-1,-1\rangle].\end{aligned} \tag{25}$$

It is important to observe that in the case of perpendicular excitation both e labeled ($J=l\pm1$) as well as f labeled ($J=l$) states are prepared, whereas in the case of parallel excitation, only e-labeled states are prepared. The simultaneous preparation of both e- and f-labeled states can be understood easily within a case (a) description. For a molecule in a ${}^1\Pi$ electronic state, the electronic wave function is *symmetric* with respect to reflection in the plane of rotation of the molecule for the e-labeled ($\epsilon=+1$) component of the

Π state Λ doublet, denoted $\Pi(A')$ levels, and *antisymmetric* for the *f*-labeled ($\epsilon = -1$) Λ doublet, denoted $\Pi(A'')$ levels.[45] The plane of rotation here is just the collision plane. As we see clearly in Fig. 6, for perpendicular excitation an initially excited *p* orbital can be both symmetric or antisymmetric with respect to reflection of the wave function in the collision plane. Hence both the *e* and *f* components of the $^1\Pi$ state are prepared.

In the case of perpendicular excitation, an adiabatic analysis will involve all the other singlet case (e) states which can be mixed with state $|1_\perp\rangle$ by the electrostatic Hamiltonian. Since the Hamiltonian does not couple *e* and *f* states, and since the matrix elements of the Hamiltonian in the case (e) basis are independent of M, only *four* other singlet states meet this criteria, instead of the three states in the case of parallel excitation.[46] In a manner similar to Eq. (22), these states can be written

$$|i_\perp\rangle = \{\chi_k^l\}\mathbf{C}_\perp^l, \tag{26}$$

where the 5×5 matrix $\mathbf{C}_\perp^l$ is given in Table V and where the five χ_k^l basis functions are linear combinations of case (e) states given by

$$\chi_1^l = 2^{-1/2}[-|l,J=l-1,M\rangle + |l,J=l-1,-M\rangle], \tag{27a}$$

$$\chi_2^l = 2^{-1/2}[-|l,J=l+1,M\rangle + |l,J=l+1,-M\rangle], \tag{27b}$$

$$\chi_3^l = 2^{-1/2}[-|l+2,J=l+1,M\rangle + |l+2,J=l+1,-M\rangle], \tag{27c}$$

$$\chi_4^l = 2^{-1/2}[-|l-2,J=l-1,M\rangle + |l-2,J=l-1,-M\rangle], \tag{27d}$$

$$\chi_5^l = 2^{-1/2}[|l,J=l,M\rangle + |l,J=l,-M\rangle]. \tag{27e}$$

Since χ_5 is the only *f* labeled state in the $\{\chi_k^l\}$ basis and since $(\mathbf{C}_\perp^l)_{51} = 2^{-1/2}$, the initially prepared state $|1_\perp\rangle$ is an equal mixture of *e*- and *f*-labeled states, as anticipated. This initially prepared state is now degenerate at long range with *two* of the other states (instead of one in the case of parallel excitation). These two states can be expressed in an uncoupled basis as

$$|2_\perp\rangle = 2^{-1/2}[-|j,m_j=0\rangle|l,m_l=1\rangle + |j,m_j=0\rangle|l,m_l=-1\rangle], \tag{28b}$$

$$|3_\perp\rangle = 2^{-1/2}[-|j,m_j=-1\rangle|l,m_l=2\rangle + |j,m_j=1\rangle|l,m_l=-2\rangle]. \tag{28c}$$

Compared to state $|1_\perp\rangle$, states $|2_\perp\rangle$, and $|3_\perp\rangle$ correspond to a reorientation of both the *p* orbital as well as the orbital angular momentum. As in the case of parallel excitation, the presence of states with both $m_j = 0$ and $m_j = \pm 1$ as members of this degenerate triplet implies that as soon as R becomes small enough that the Σ and Π electrostatic potentials begin to differ significantly, the initially prepared orientation of the *p* orbital may be lost.

Diagonalization of the matrix of the Hamiltonian in the $|i_\perp\rangle$ basis will yield four *e*-labeled and one *f*-labeled adiabatic states. The energies of the four *e*-labeled states will be *identical* to those in the case of parallel excitation, since the matrix elements of the electrostatic potential [Eq. (8)] are independent of M. As R decreases, these curves separate into two pairs, which correlate at short range with, respectively, the $^1W_\Sigma(R)$ and $^1W_\Pi(R)$ curves in Fig. 1. The sole *f*-labeled state will follow the $^1W_\Pi(R)$ curve.

V. STATISTICAL MODEL FOR THE POLARIZATION DEPENDENCE OF $^1P\rightarrow{}^3P$ CROSS SECTIONS

We can use the discussion in the preceding section to construct a simple model for the observed dependence of the $^1P\rightarrow{}^3P$ cross sections on the direction of polarization of the pump laser. In the case of parallel excitation, only *e*-labeled states are involved and the initially prepared state correlates with equal probability at short range with a Π-like and a Σ-like curve. A simple statistical model would then predict, in the absence of any knowledge of how the incoming flux is distributed between these two curves, that for parallel excitation the probability of accessing either the $^1\Sigma$ or the $^1\Pi$ curve is 0.5. On the other hand, in the case of perpendicular excitation, the initially prepared state is an equal mixture of *e*- and *f*-labeled states. At short range the *e* components of this initially prepared state correlate equally with a Π-like and a Σ-like curve while the single *f* component correlates just with the $^1\Pi(A'')$ curve. Thus, under perpendicular excitation the probability of accessing a Σ-like curve is 0.25 and the probability of accessing a Π-like curve [either $^1\Pi(A')$ or $^1\Pi(A'')$] is 0.75.

Now, suppose that the probability of undergoing this $^1P\rightarrow{}^3P$ transition if P_Π from the $^1\Pi$ curve and P_Σ from the $^1\Sigma$ curve. Then the ratio of the $^1P\rightarrow{}^3P$ cross sections under parallel versus perpendicular excitation will be

$$\sigma_\perp/\sigma_\parallel = (0.75P_\Pi + 0.25P_\Sigma)/(0.5P_\Pi + 0.5P_\Sigma). \tag{29}$$

Let us consider three limiting cases. The first, $P_\Sigma = 0$, would be reasonable if the alkaline earth–noble gas potential curves had the form of those in Fig. 1, where the singlet–triplet crossing is accessible only by a crossing between the $^1\Pi$ and $^3\Sigma$ curves. In this case the cross-section ratio would be $\sigma_\perp/\sigma_\parallel = 1.5$. The second limiting case, $P_\Pi = 0$, would be reasona-

TABLE V. Transformation matrix $\mathbf{C}_\perp^l$ for perpendicular excitation.

$\{(l-1)/2(2l+1)\}^{1/2}$	$-\{(l-1)(l+1)/l(2l+1)\}^{1/2}$	$\{(l+1)(l+2)/2l(2l+1)\}^{1/2}$	0	0
$-\{(l+2)/2(2l+1)\}^{1/2}$	$\{l(l+2)/(l+1)(2l+1)\}^{1/2}$	$\{l(l-1)/2(l+1)(2l+1)\}^{1/2}$	0	0
0	0	0	1	0
0	0	0	0	1
$-2^{-1/2}$	$\{l(l+1)\}^{-1/2}$	$\{(l+2)(l-1)/2l(l+1)\}^{1/2}$	0	0

ble if the alkaline earth–noble gas potential curves had the form of those in Fig. 8, where the singlet–triplet transitions can occur by a crossing at long range between the $^1\Sigma$ and $^3\Pi$ curves. In this case the cross-section ratio would be $\sigma_\perp/\sigma_\parallel = 0.5$. In the third limiting case, the singlet–triplet crossing will be accessible with equal probability from both the $^1\Sigma$ and $^1\Pi$ curves ($P_\Sigma = P_\Pi$). In this case the $^1P \rightarrow {}^3P$ cross section would be independent of the direction of laser polarization and the cross section ratio would equal unity.

VI. INWARD PROPAGATION WITH ADIABATIC PROJECTION

The simple statistical model presented above ignores any dynamical effects, and, in particular, assumes that as the Ca atom in the initially prepared ^1P state approaches the collision partner, all incoming flux will be distributed equally among the two $^1\Pi_e$ and two $^1\Sigma_e$ states which are coupled with the initially prepared state ($1_\parallel$ or $1_\perp$). By determining the distribution of flux among these adiabatic states as a function of internuclear separation we can assess the validity of this statistical model. We proceed as follows.

In the case of parallel excitation in the short range region the scattering wavefunction can be expressed as a linear combination of the four e-labeled adiabatic states obtained by diagonalization of the Hamiltonian in the case (e) basis defined by Eqs. (21). Following Eq. (17), we designate these e-labeled adiabatic states as $|nJM;R\rangle$ [Eq. (17)], where $n = 1$–4. To determine the distribution of flux among these adiabatic states at $R = R_{\min}$, say, we shall first write the total scattering wave function at $R_{\min}$ as a set of four linearly independent solutions, namely[47]

$$\Psi(R_{\min}) = \frac{1}{R_{\min}} \mathbf{G}(R_{\min}), \tag{30}$$

where $\mathbf{G}(R)$ is a diagonal matrix with elements

$$G_{ij} = \delta_{ij} k_i^{-1/2} \exp[-ik_i(R_{\min})R] \quad \text{if } \lambda_i^J(R_{\min}) < E, \tag{31a}$$

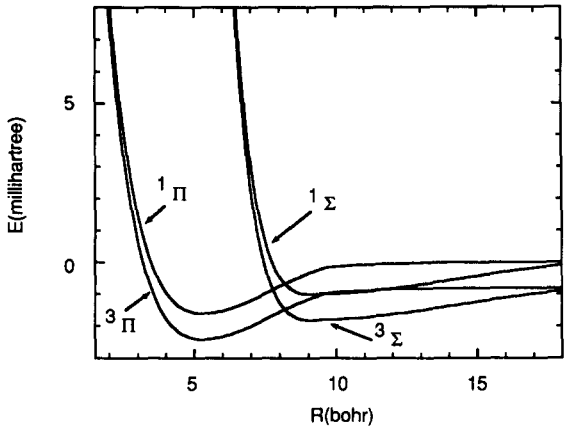

FIG. 8. Potential-energy curves of $^1\Sigma$, $^3\Sigma$, $^1\Pi$, and $^3\Pi$ symmetry which would arise from the interaction of a strongly polarizable atom with an atom in ($...nsn'p\ ^1P$) and ($...nsn'p\ ^3P$) electronic states. As contrasted to the curves displayed in Fig. 1, here the stronger and deeper well in the curves of Σ symmetry causes the $^1\Sigma$–$^3\Pi$ crossing to occur at longer range than the $^1\Pi$–$^3\Sigma$ crossing. The actual potential-energy curves shown are those used for the calculation of $^1P \leftrightarrow {}^3P$ cross sections for the collision of Ca($4s5p$) with Xe (Ref. 55).

$$G_{ij} = \delta_{ij} k_i^{-1/2} \exp[k_i(R_{\min})R] \quad \text{if } \lambda_i^J(R_{\min}) > E. \tag{31b}$$

Here $\lambda_i^J(R)$ is the adiabatic energy of the ith adiabatic state [Eq. (18)] and k_i is the corresponding wave vector, namely

$$k_i(R) = [2\mu|E - \lambda_i^J(R)|/\hbar^2]^{1/2}. \tag{32}$$

These boundary conditions correspond to an incoming wave in each adiabatic channel which is energetically open at $R = R_{\min}$, and an exponentially decaying function in each adiabatic channel which is energetically closed.

We then transform this set of linearly independent solutions into the asymptotic, case (e) basis,

$$\mathbf{F}(R_{\min}) = \mathbf{A}_\parallel^T(R_{\min})\mathbf{G}(R_{\min},r), \tag{33}$$

where the matrix $\mathbf{A}_\parallel$ is the transformation from the adiabatic to case (e) basis [Eqs. (17)]. After propagation to a large value of R, this set of solutions is matched at a value of $R = R_{\max}$, which lies beyond the range of the electrostatic interaction $W(R_{\max},\mathbf{r})$ [Eq. (3)], to scattering boundary conditions in terms of Riccati–Hankel functions[48,49]

$$\mathbf{F}(R_{\max}) = -i[\hat{\mathbf{h}}^{(2)}(R_{\max}) + \hat{\mathbf{h}}^{(1)}(R_{\max})\mathbf{S}]. \tag{34}$$

Here $\hat{\mathbf{h}}^{(m)}(R)$ is a diagonal matrix with elements proportional to Ricatti–Hankel functions, which are sums of the real Ricatti–Bessel functions of the first kind,[48] namely

$$[\hat{\mathbf{h}}^{(m)}(R)]_{ij} = \delta_{ij} k_i^{-1/2}[\hat{j}_l(k_iR) - i(-1)^{(m)}\hat{y}_l(k_iR)], \tag{35}$$

with k_i denoting here the asymptotic value of the wave vector. In Eq. (34) $\mathbf{S}$ designates the scattering matrix.

For the particular combination of case (e) functions which is initially prepared in the experiments of Leone and co-workers (states $|1_\parallel\rangle$ or $|1_\perp\rangle$ defined in Sec. V), the asymptotic form of the scattering wave function corresponding to incoming flux in the initially prepared state is given by

$$\mathbf{F}_\parallel(R_{\max}) = \mathbf{F}(R_{\max})\mathbf{c}_\parallel = -i[\hat{\mathbf{h}}^{(2)}(R_{\max}) + \hat{\mathbf{h}}^{(1)}(R_{\max})\mathbf{S}]\mathbf{c}_\parallel, \tag{36}$$

where $\mathbf{c}_\parallel$ designates the first column of the transformation matrix $\mathbf{c}_\parallel$ defined by Eq. (23) (Table III). At $R = R_{\min}$, the corresponding scattering wave function in the asymptotic, case (e) basis is then given by $\mathbf{F}(R_{\min})\mathbf{c}_\parallel$ and, in the adiabatic basis, by

$$\mathbf{g}_\parallel(R_{\min}) = \mathbf{A}_\parallel(R_{\min})\mathbf{F}(R_{\min})\mathbf{c}_\parallel = \mathbf{G}(R_{\min})\mathbf{c}_\parallel. \tag{37}$$

Note that for a particular choice of initial conditions (incoming flux in state $|1_\parallel\rangle$ or $|1_\perp\rangle$) the scattering wave function is a column vector, rather than a matrix; this is denoted by using lower case g. The flux in adiabatic state $|n\rangle$ at $R = R_{\min}$ is just

$$\mathbf{J}_n = -(\hbar/\mu)|[\mathbf{g}_\parallel(R_{\min})]_n|^2. \tag{38}$$

As will be discussed in the Appendix a log-derivative propagation scheme[50–52] was used to obtain the S matrix and the wave function at $R_{\min}$.

In the case of perpendicular polarization in the short-range region the scattering wave function can be expressed as a linear combination of the five adiabatic states obtained

by diagonalization of the Hamiltonian in the case (e) basis defined by Eq. (27). The distribution of incoming flux among these adiabatic states at $R_{\min}$ is determined exactly as above, with Eq. (37) replaced by

$$\mathbf{g}_\perp(R_{\min}) = \mathbf{A}_\perp(R_{\min})\mathbf{F}(R_{\min})\mathbf{c}_\perp = \mathbf{G}(R_{\min})\mathbf{c}_\perp, \quad (39)$$

where $\mathbf{c}_\perp$ is the first column of the transformation matrix $\mathbf{C}_1^J$ defined by Eq. (26) (Table V).

We have used this technique of inward propagation with adiabatic projection to follow the distribution of flux associated with the initially prepared states in the case of both parallel and perpendicular polarization. For parallel excitation the upper panel in Fig. 9 displays the ratio of the flux into the two adiabatic states which correlate at short range with Σ-like curves as compared to the flux into the two adiabatic states which correlate at short range with Π-like curves (see Fig. 7). These calculations were based on the Σ and Π curves of Fig. 1 with a collision mass corresponding to Ca + He and at an energy of 0.067 eV (2.5 millihartree). Curves are displayed for three values of the initial nuclear orbital angular momentum: $l = 3$, 10, and 40. In the purely statistical limit (Sec. V) this flux ratio would be unity. We observe that at large R, there is some deviation from statistical behavior and some variation with R of the flux ratio. The structure at $R \approx 13$ bohr corresponds to the point at which the splitting between the Σ and Π electrostatic energies passes through zero (see the inset panel in Fig. 7). However, at shorter distances, and, in particular, as the system approaches the curve crossing with the lower $^3\Sigma^+$ state (Figs. 2 and 3) the flux ratio becomes extremely close to the statistical limit of unity; by this value of R the flux in the initially prepared $|1_\parallel\rangle$ state has become equally apportioned between the Σ-like and Π-like adiabatic states.

We observe that in the case of the highest orbital angular momentum shown ($l = 40$), the flux ratio drops precipitously to zero at $R \approx 8.75$ bohr. The centrifugal barrier associated with this value of l is so large that the classical turning point of the Σ-like adiabatic states occurs at $R \approx 8.75$ bohr. At this point all the flux on the Σ curves is reflected.

In the lower panel of Fig. 9 we display, for the same system at the same energy, the ratio of the flux into the Π-like adiabatic states in the case of perpendicular, as opposed to parallel, excitation. Again, curves are shown for three values of the initial nuclear orbital angular momentum. As before, the structure at $R = 13$ bohr reflects the crossing at long range between the Σ and Π electrostatic curves. At shorter values of R, the flux ratio approaches closely the statistical limit of 1.5. We recall that flux into the Π-like adiabatic states will be larger in the case of perpendicular excitation because 50% of the initially excitation occurs into f-labeled states, which can correlate at short range only with Π-like adiabatic states.

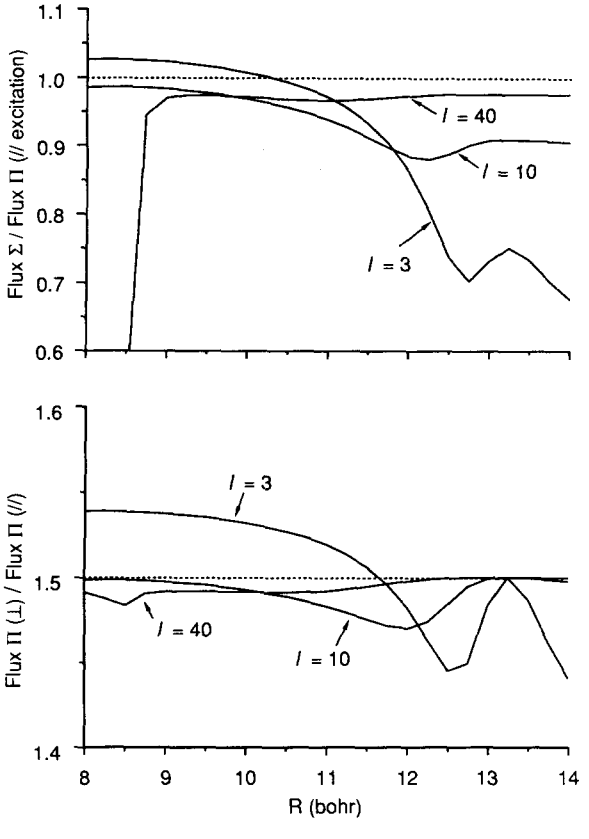

FIG. 9. (Upper panel) Ratio of flux into the $^1\Sigma$-like adiabatic states against flux into the $^1\Pi$-like adiabatic states as a function of the internuclear distance in the case of parallel excitation, for three different values of the initial nuclear rotational angular momentum l. Due to the large centrifugal barrier for $l = 40$ the turning point in the $^1\Sigma$-like adiabatic states occurs at $R \approx 9$. For values of R less than this value there is no flux into the $^1\Sigma$-like adiabatic states, hence the sharp drop in the curve. The dashed curve indicates the ratio predicted by the statistical model of Sec. V. (Lower panel) Ratio of flux into the $^1\Pi$-like diabatic states as a function of the internuclear distance in the case of perpendicular excitation as opposed to parallel excitation, for three different values of the initial nuclear rotational angular momentum l. The dashed curve indicates the ratio predicted by the statistical model of Sec. V.

VII. ORBITAL LOCKING MODELS

The initial experiments of Leone and co-workers $^1P \rightarrow {}^3P$ transitions in collisions of electronically excited alkaline earth atoms[2–5] and those of Rettner and Zare on reactive collisions of Ca($4s4p\ ^1P$)[1] were interpreted using the concept of "orbital locking."[10–12] This model was developed by Hertel and co-workers[10–12] to interpret earlier experimental work on collisions involving electronically excited Na atoms in ^2P states. Within this model it is assumed that if the pump laser initially excites a p orbital either lying along, or perpendicular to, **R**, the orientation of the orbital with respect to **R** will remain fixed or "frozen" with respect to a space-frame coordinate system at large values of R but will "follow" **R** once the atoms have approached within a certain distance, designated the "locking radius." If the initially excited p orbital perfectly follows **R**, then perpendicular excitation will result in a π orientation of the p orbital at close range (p orbital perpendicular to **R**), while parallel excitation will result in a σ orientation (p orbital parallel to **R**). The reverse will occur if the initially excited p orbital remains frozen: perpendicular excitation will lead to σ orientation and parallel excitation, to π orientation.

This analysis is conceptually and pictorially appealing. It can also be used to provide a qualitatively satisfactory interpretation of the experimental results of Leone and co-

workers,[2–5] as follows: In cases where the $^1\Pi$–$^3\Sigma$ crossing (Fig. 1) provides the means for $^1P \rightarrow {}^3P$ transfer, if orbital locking occurs then one would observe an enhancement of the $^1P \rightarrow {}^3P$ cross section under perpendicular excitation.

Unfortunately, our earlier exact quantum study of the Ca($4s5p$) + He system revealed that the region of strong nonadiabatic mixing which characterized the transition from a case (e) to case (a) basis occurred over a sizeable region of internuclear separation, rather than at a specific value of R. The quantum analysis presented here reveals several additional flaws in the orbital locking model.

As we have seen in the preceding two sections, at long range the initially prepared state, both for parallel as well as perpendicular excitation, is degenerate with one (or more) states which differ only by reorienting both m_L and m_l by ± 1 unit of angular momentum, so that the total projection quantum number remains constant. As a result an initially prepared e labeled state, in which the space or laboratory frame orientation of the atomic p orbital is well defined, becomes an equal mixture of the degenerate levels, with a consequent loss of information about the space-frame orientation of **L**. Actual calculation of the distribution of flux as a function of internuclear separation (previous section) revealed the initial flux divides virtually identically between states which followed Σ-like curves at short range and states which followed Π-like curves. Thus for the e-labeled states the degree of orbital "locking" is independent of the initial state preparation.

The important difference between parallel and perpendicular excitation is that in the latter case, 50% of the initially prepared states are f-labeled states in which the p orbital lies perpendicular to the plane of the collision. Since these f-labeled states cannot mix with states which follow Σ-like curves at short range, for perpendicular excitation the initially prepared orbital must remain frozen 50% of the time and thus can never "lock" onto the internuclear axis, even at distances shorter than the "locking radius." In terms of a case (a) analysis, perpendicular excitation produces equal populations in both the $\Pi(A')$ and $\Pi(A'')$ Λ doublets. Only the $\Pi(A')$ states can mix with the $^1\Sigma$ state.

VIII. CONCLUSION

We have presented here a detailed review of the fully quantum description of inelastic collisions involving atoms in ^1P electronic states. We have stressed the following.

(1) How various Hund's case coupling schemes can help to clarify the interactions and couplings which are present and to make simple predictive models for alignment effects.

(2) The care which must be used in describing correctly the initial state in beam experiments involving laser excitation.

(3) How the study of the distribution of initial flux among the accessible adiabatic states can be used to establish the validity of simple mechanistic and statistical models. As an example of the insight gained we cite the case of perpendicular excitation, where, contrary to what one might guess, the initially excited orbital is not constrained to be perpendicular to the collision plane. This is understandable from the viewpoint of a Hund's case (a) description: a $^1\Pi$ state has both A' and A'' Λ doublets, in which the electronic wave functions are, respectively, *symmetric* and *antisymmetric* with respect to reflection in the plane of rotation of the molecule.[45] As another example of the use of a case (a) description, it is well known to spectroscopists that the **J·L** term in the rotational Hamiltonian will mix nearly degenerate $^1\Pi$ and $^1\Sigma$ states.[15] This implies that a p orbital initially oriented parallel (Σ) to the relative velocity vector will rapidly scramble and become mixed with the e-labeled Π state in which the p orbital lies perpendicular to **R**.

As stressed in the preceding section, any simple, mechanistic model of the spin–changing transitions under study here must be consistent with the full quantum description. The development of orbital locking models[10–12] was prompted by a desire to understand exactly how the initially prepared state evolves, both for parallel and perpendicular excitation. We have shown here that this knowledge can be gained in a straightforward manner, by propagation of the wave function corresponding to a properly defined initial state, projecting it onto the adiabatic basis as a function of the internuclear distance, and then determining the flux in each adiabatic state. Numerical calculations showed that irrespective of the polarization of the initial excitation, the flux associated with states which are symmetric with respect to reflection in the plane of rotation of the Ca–M system become completely mixed, at distances beyond the singlet-triplet crossing which is responsible for the observed $^1P \rightarrow {}^3P$ transitions. The present paper confirms explicitly the state scrambling which we put forth as an interpretation of our earlier quantum scattering studies on the Ca($4s5p$) + He system.[9]

Guided by our analysis in terms of Hund's case coupling schemes and by the observed complete scrambling of flux among the A' states, we developed the following simple statistical model for prediction of the polarization dependence of cross sections for $^1P \rightarrow {}^3P$ transitions: In cases where $^1P \rightarrow {}^3P$ transfer is facilitated predominately by a crossing between the $^1\Pi$ and $^3\Sigma$ curves (Fig. 1), the ratio of the cross sections for perpendicular as compared to parallel excitation should be 1.5. By contrast, in cases where $^1P \rightarrow {}^3P$ transfer is facilitated predominately by a crossing between the $^1\Sigma$ and $^3\Pi$ curves (Fig. 8), the ratio of the cross sections for perpendicular as compared to parallel excitation should fall to 0.5.

The ideas and methods presented here should certainly be extended to deal with encounters between an electronically excited atom and a molecule. The situation will be more complicated in that the doubly degenerate Π potential curves of the two atom system will be replaced by two potential-energy surfaces, of A' and A'' symmetry in c_s geometry. Similarly the Σ potential curve of the two atom system will itself become a surface of A' symmetry. A formally equivalent situation, collisions of $F(^2P)$ with H_2, has been treated by Rebentrost and Lester.[53]

However, despite the additional complexity, it is clear that the same scrambling of the initially prepared orbital orientation will occur in atom–molecule collisions. For example, in the case of parallel excitation one of the A' wave

functions will be prepared which can subsequently mix with the other, degenerate A' wave function. In the case of a molecular partner this mixing will be induced not only by the splitting between the two A' potential-energy surfaces as a function of the atom–molecule separation (as in the case of atom–atom collisions) but also by the variation in this splitting as the orientation of the molecule with respect to **R** changes.

The major impediment to calculations of cross sections or studies of initial flux redistribution in collisions of, for example, Ca($4s5p\ ^1P$) with a molecule is the total lack of information on the necessary *six* potential-energy surfaces (two A' and one A'' surfaces of both singlet and triplet multiplicity) plus the additional off-diagonal coupling matrix elements in a diabatic basis[53,54] which arise in collisions involving a molecular partner. In the case of atomic collisions it is easily possible to carry out a series of calculations based on qualitatively reasonable model potentials.[9] By varying the parameters on which these potentials depend one can explore[9,55] which features of the potential-energy curves are probed experimentally. This type of study will be much more difficult in the case of a molecular partner.

Note added in proof: Recently, Schatz, Kovalenko, and Leone have developed an alternative interpretation of the evolution, in collisions with noble gases, of ^2P state atoms prepared initially with either parallel or perpendicular excitation. Within their interpretation, which is based on an initial J, rather than initial l (as used in the present article) formulation, a considerable degree of orbital "following" can occur. Thus the statistical scrambling of the initial orbital alignment seen, for example, in Fig. 9, would be the consequence of the neglect of interference between the various initial l states in the incoming plane wave.

ACKNOWLEDGMENTS

The authors would like to acknowledge their debt to the U. S. Army Research Office under Grant No. DAAG29-85-K-0018. They have also benefitted from the encouragement and stimulating criticism of S. Leone, I. Hertel, J. Delos, and L. Kovalenko. B. P. is grateful to M. Child for several helpful discussions. M. H. A. would like to thank D. Clary for conversations which inspired the idea of projecting the propagated wave function onto locally adiabatic states.

APPENDIX: DETERMINATION OF SCATTERING WAVE FUNCTION

We use a log-derivative propagation scheme to determine the S matrix and scattering wave function (Sec. II). For more details we refer the reader to the papers of Mrugala and Secrest[51] and Manolopoulos.[52] Consider two values of the internuclear separation R_a and R_b, with $R_b > R_a$. We designate the scattering wave function by $\mathbf{F}(R)$ and its derivative with respect to R by $\mathbf{F}'(R)$. Both $\mathbf{F}(R)$ and $\mathbf{F}'(R)$ are square matrices of dimension equal to the number of channels N. Within a log-derivative propagation scheme the wave function and its derivative at R_a and R_b are related by the matrix equation[51,52]

$$\begin{bmatrix}\mathbf{F}'(R_a)\\ \mathbf{F}'(R_b)\end{bmatrix}=\begin{bmatrix}\mathbf{L}_1(a,b) & \mathbf{L}_2(a,b)\\ \mathbf{L}_3(a,b) & \mathbf{L}_4(a,b)\end{bmatrix}\begin{bmatrix}-\mathbf{F}(R_a)\\ \mathbf{F}(R_b)\end{bmatrix}, \quad \text{(A1)}$$

where the log-derivative propagators $\mathbf{L}_i(a,b)$ are $N\times N$ matrices. The log-derivative matrix is defined by

$$\mathbf{Y}(R)=\mathbf{F}'(R)\mathbf{F}(R)^{-1}. \quad \text{(A2)}$$

From Eqs. (A1) and (A2) one can show that the log-derivative matrix at R_b can be expressed in terms of the log-derivative matrix at R_a as

$$\mathbf{Y}(R_b)=\mathbf{L}_4(a,b)-\mathbf{L}_3(a,b)\times[\mathbf{Y}(R_a)+\mathbf{L}_1(a,b)]^{-1}\mathbf{L}_2(a,b). \quad \text{(A3)}$$

It then follows that

$$\mathbf{F}(R_a)\mathbf{F}(R_b)^{-1}=[\mathbf{Y}(R_a)+\mathbf{L}_1(a,b)]^{-1}\mathbf{L}_2(a,b). \quad \text{(A4)}$$

From Eqs. (17), (31), and (A2) we observe that the log-derivative matrix in the asymptotic case (e) basis at $R_{\min}$ is given by

$$\mathbf{Y}(R_{\min})=\mathbf{A}^T(R_{\min})\mathbf{y}(R_{\min})\mathbf{A}(R_{\min}), \quad \text{(A5)}$$

where $\mathbf{y}(R_{\min})$, the log-derivative matrix in the adiabatic basis at $R_{\min}$, is a diagonal matrix with elements

$$y(R_{\min})_{ij}=\delta_{ij}k_i(R_{\min}) \quad \text{if } \lambda_i^J(R_{\min})>E \quad \text{(A6)}$$

and

$$y(R_{\min})_{ij}=-i\delta_{ij}k_i(R_{\min}) \quad \text{if } \lambda_i^J(R_{\min})<E, \quad \text{(A7)}$$

where the local wave vectors $k_i(R)$ are defined by Eq. (32).

By repeated application of Eq. (A3) one determines the log-derivative matrix at $R_{\max}$, from which the S matrix can be obtained as

$$\mathbf{S}=[\hat{\mathbf{h}}^{(1)\prime}(R_{\max})-\mathbf{Y}(R_{\max})\hat{\mathbf{h}}^{(1)}(R_{\max})]^{-1}\times[\mathbf{Y}(R_{\max})\hat{\mathbf{h}}^{(2)}(R_{\max})-\hat{\mathbf{h}}^{(2)\prime}(R_{\max})], \quad \text{(A8)}$$

where the primes denote differentiation with respect to R and the diagonal matrices $\hat{\mathbf{h}}^{(m)}$ are defined by Eq. (35). Simultaneous with propagation of the log-derivative matrix we construct, by repeated application of Eq. (A4) the matrix

$$\mathbf{F}(R_{\min})\mathbf{F}(R_{\max})^{-1}=\mathbf{F}(R_{\min})\mathbf{F}(R_b)^{-1}\mathbf{F}(R_b)\mathbf{F}(R_c)^{-1}\cdots\mathbf{F}(R_y)\mathbf{F}(R_z)^{-1}\mathbf{F}(R_z)\mathbf{F}(R_{\max})^{-1}, \quad \text{(A9)}$$

which allows us to construct the scattering wave function at $R_{\min}$ from $\mathbf{F}(R_{\max})$ [Eq. (36)].

In our implementation of this log-derivative propagation scheme we used the modified Simpson's rule approximation[52] to the log-derivative propagators suggested originally by Johnson.[50]

[1] C. T. Rettner and R. N. Zare, J. Chem. Phys. **74**, 3630 (1981); **77**, 2417 (1982).
[2] M. O. Hale and S. R. Leone, J. Chem. Phys. **79**, 3352 (1983).
[3] M. O. Hale, I. V. Hertel, and S. R. Leone, Phys. Rev. Lett. **53**, 2296 (1984).
[4] D. Neuschäfer, M. O. Hale, I. V. Hertel, and S. R. Leone, in *Electronic and Atomic Collisions*, edited by D. C. Lorents, W. E. Meyerhof, and J. R. Peterson (North-Holland, Amsterdam, 1985), p. 585; W. Bussert, D.

Neuschäfer, and S. R. Leone, J. Chem. Phys. **87**, 3833 (1987).
[5]S. R. Leone, in *Selectivity in Chemical Reactions*, edited by J. C. Whitehead (Kluwer Academic, Dordrecht, 1988), p. 245.
[6]W. Bussert and S. R. Leone, Chem. Phys. Lett. **138**, 269 (1987).
[7]R. W. Schwenz and S. R. Leone, Chem. Phys. Lett. **133**, 433 (1987); W. Bussert and S. R. Leone, *ibid.* **138**, 276 (1987).
[8]A. Z. Devdariani and A. L. Zagrebin, Chem. Phys. Lett. **131**, 197 (1986).
[9]B. Pouilly and M. H. Alexander, J. Chem. Phys. **86**, 4790 (1987).
[10]H. W. Hermann and I. V. Hertel, Comments At. Mol. Phys. **12**, 61, 127 (1982).
[11]I. V. Hertel, H. Schmidt, A. Bähring, and E. Meyer, Rep. Prog. Phys. **48**, 375 (1985).
[12]R. Witter, E. E. B. Cambell, C. Richter, H. Schmidt, and I. V. Hertel, Z. Phys. D **5**, 101 (1987).
[13]G. Herzberg, *Molecular Spectra and Molecular Structure. I. Spectra of Diatomic Molecules* (Van Nostrand, Princeton, NJ, 1950).
[14]J. T. Hougen, Natl. Bur. Stand. (U.S.) Monogr. 115 (1970).
[15]H. Lefebvre-Brion and R. W. Field, *Perturbations in the Spectra of Diatomic Molecules* (Academic, New York, 1986).
[16]E. E. Nikitin, J. Chem. Phys. **43**, 744 (1965); Adv. Chem. Phys. **28**, 317 (1975); E. E. Nikitin and S. Ya. Umanskii, *Theory of Slow Atomic Collisions* (Springer-Verlag, Berlin, 1984).
[17]E. I. Dashevskaya, E. E. Nikitin, and A. I. Reznikov, J. Chem. Phys. **53**, 1175 (1970).
[18]F. Masnou-Seeuws and R. MacCarroll, J. Phys. B **7**, 2330 (1974).
[19]V. Aquilanti and G. Grossi, J. Chem. Phys. **73**, 1165 (1980); V. Aquilanti, P. Casavecchia, G. Grossi, and A. Laganá, *ibid.* **73**, 1173 (1980); V. Aquilanti, G. Grossi, and A. Laganá, Nuovo Cimento **63B**, 7 (1981).
[20]M. H. Alexander, T. Orlikowski, and J. E. Straub, Phys. Rev. A **28**, 73 (1983).
[21]B. Pouilly, T. Orlikowski, and M. H. Alexander, J. Phys. B **18**, 1953 (1985).
[22]D. Lemoine, J.-M. Robbe, and B. Pouilly, J. Phys. B **21**, 1007 (1988).
[23]M. H. Alexander and B. Pouilly, in *Selectivity in Chemical Reactions*, edited by J. C. Whitehead (Kluwer Academic, Dordrecht, 1988), p. 265.
[24]R. H. G. Reid, J. Phys. B **6**, 2018 (1973).
[25]F. H. Mies, Phys. Rev. A **7**, 942 (1973).
[26]D. M. Brink and G. R. Satchler, *Angular Momentum*, 2nd ed. (Clarendon, Oxford, 1975).
[27]J. M. Brown, J. T. Hougen, K.-P. Huber, J. W. C. Johns, I. Kopp, H. Lefebvre-Brion, A. J. Merer, D. A. Ramsay, J. Rostas, and R. N. Zare, J. Mol. Spectrosc. **55**, 500 (1975).
[28]R. P. Saxon, R. E. Olson, and B. Liu, J. Chem. Phys. **67**, 2692 (1977).
[29]B. Pouilly, B. H. Lengsfield, and D. R. Yarkony, J. Chem. Phys. **80**, 5089 (1984).
[30]J. Pascale and M. Y. Perrin, J. Phys. B **13**, 1839 (1980), J. Pascale, Phys. Rev. A **28**, 632 (1983).
[31]R. N. Zare, A. L. Schmeltekopf, W. J. Harrop, and D. L. Albritton, J. Mol. Spectrosc. **46**, 37 (1973).
[32]M. Larsson, Phys. Scr. **23**, 835 (1981).
[33]A. M. Arthurs and A. Dalgarno, Proc. R. Soc. London **A256**, 540 (1960).
[34]R. H. G. Reid and A. Dalgarno, Phys. Rev. Lett. **22**, 1029 (1969); Chem. Phys. Lett. **6**, 85 (1970).
[35]A. D. Wilson and Y. Shimoni, J. Phys. B **7**, 1543 (1974); **8**, 1392, 2393 (1975).
[36]R. E. Olson, Chem. Phys. Lett. **33**, 250 (1975).
[37]A. I. Voronin and V. A. Kvilividze, Theor. Chim. Acta. **8**, 334 (1967).
[38]R. K. Preston, C. Sloane, and W. H. Miller, J. Chem. Phys. **60**, 4961 (1974).
[39]M. S. Child, *Molecular Collision Theory* (Academic, New York, 1974).
[40]F. H. Mies, Mol. Phys. **41**, 973 (1980).
[41]E. U. Condon and G. H. Shortley, *The Theory of Atomic Spectra* (Cambridge University, Cambridge, England, 1951).
[42]S. Geltman, *Topics in Atomic Collision Theory* (Academic, New York, 1969).
[43]G. G. Balint-Kurti, in Theoretical Chemistry, *MTP International Review of Science, Physical Chemistry, Series 2* (Butterworths, London, 1975), Vol. I.
[44]As the collision energy increases, the orbital angular momentum corresponding to a given value of the impact parameter will increase. Since the coupling between states $|1_{\|}\rangle$ and $|2_{\|}\rangle$ decreases as $1/l$, the error introduced by neglect of the reorientation of l will become less significant in the high-energy limit.
[45]M. H. Alexander, P. Andresen, R. Bacis, R. Bersohn, F. J. Comes, P. J. Dagdigian, R. N. Dixon, R. W. Field, G. W. Flynn, K.-H. Gericke, E. R. Grant, B. J. Howard, J. R. Huber, D. S. King, J. L. Kinsey, K. Kleinermanns, K. Kuchitsu, A. C. Luntz, A. J. McCaffery, B. Pouilly, H. Reisler, S. Rosenwaks, E. W. Rothe, M. Shapiro, J. P. Simons, R. Vasudev, J. R. Wiesenfeld, C. Wittig, and R. N. Zare, J. Chem. Phys. **89**, 1749 (1988).
[46]The number of states which are coupled to the initially prepared state in the case of perpendicular polarization was incorrectly overestimated in Refs. 9 and 23.
[47]See, for example, D. Secrest, in *Atom-Molecule Collision Theory. A Guide for the Experimentalist*, edited by R. B. Bernstein (Plenum, New York, 1979).
[48]M. Abramowitz and I. Stegun, Natl. Bur. Stand. Appl. Math. Ser. 55 (1965), Sec. 10.3.
[49]Since

$$\lim_{x\to\infty} \hat{h}_l^{(1)}(kx) = -ik^{-1/2}\exp[i(kx - l\pi/2)]$$

and

$$\lim_{x\to\infty} \hat{h}_l^{(2)} = ik^{-1/2}\exp[-i(kx - l\pi/2)]$$

(Ref. 48), the boundary conditions in Eq. (34) are entirely equivalent to the usual expression (Ref. 47) in terms of $\exp[\pm i(kx - l\pi/2)]$.
[50]B. R. Johnson, J. Comp. Phys. **13**, 445 (1973).
[51]F. Mrugala and D. Secrest, J. Chem. Phys. **78**, 5954 (1983); **79**, 5960 (1983).
[52]D. Manolopoulos, J. Chem. Phys. **85**, 6425 (1986); thesis, University of Cambridge, United Kingdom, 1988.
[53]F. Rebentrost and W. A. Lester, Jr., J. Chem. Phys. **64**, 2879 (1976); **67**, 3367 (1977).
[54]M. H. Alexander and G. C. Corey, J. Chem. Phys. **84**, 100 (1986).
[55]B. Pouilly, J.-M. Robbe, and M. H. Alexander, J. Chem. Phys. (in press).